Hindawi
Shock and Vibration
Volume 2020, Article ID 7605683, 16 pages
https://doi.org/10.1155/2020/7605683

Research Article

Evaluation on Filter Performance of Variational Mode Decomposition and Its Application in Separating Closely Spaced Modes

Wenjing Gu and Li Zhou

State Key Laboratory of Mechanics and Control of Mechanical Structures, Nanjing University of Aeronautics and Astronautics, Nanjing 210016, China

Correspondence should be addressed to Li Zhou; lzhou@nuaa.edu.cn

Received 15 December 2019; Accepted 28 April 2020; Published 13 May 2020

Academic Editor: Stefano Manzoni

The equivalent filter characteristics of variational mode decomposition (VMD) are fully evaluated when applied to the fractional Gaussian noise (fGn) and the application in separating closely spaced modes of vibration system is performed in this paper. VMD is a newly proposed signal decomposition technique, which nonrecursively decomposes a signal into a given number of subsignals (modes), and each mode is mostly compact around a center pulsation. The filter performance of VMD is largely dependent on the constraint parameter and the initialization of center frequencies. In order to extract the desired modes, criteria for the determination of decomposition parameters are established. The initial center frequencies could be simply determined by prior estimated modal frequencies of the analyzed signal, while the constraint parameter is optimized utilizing a genetic algorithm (GA). A two-degree-of-freedom parametric system is considered to evaluate the capability of VMD in the separation of closely spaced modes. Compared with the noise-assisted versions of empirical mode decomposition (EMD) and wavelet packet transform (WPT), the parameter-optimized VMD can successfully separate the closely spaced modes while recovering the most modal information simultaneously. When introduced to the ground vibration test (GVT) of a horizontal tail, the proposed method successfully extracted the first five oscillation modes and identified the modal parameters accurately.

1. Introduction

Empirical mode decomposition (EMD) introduced by Huang et al. [1] is widely used to adaptively decompose a signal into separate spectral bands with different oscillation modes. EMD is a data-driven decomposition technique with a self-adaptive expansion basis and can interpret the physical meanings of data generated by nonlinear and nonstationary processes [2]. The subsignals obtained from EMD called intrinsic mode functions (IMFs) are ideally a collection of complete, adaptive, and orthogonal representation for the analyzed signal. The instantaneous modal information of each IMF thus can be derived through the Hilbert transform. Many EMD-based modal parameter identification methods have been proposed and had great impact on a variety of engineering applications [3–6].

Despite the advantages, EMD is limited by lacking thorough mathematical understandings and some other obvious shortcomings such as sensitivity to noise and sampling. Some noise-assisted versions of EMD such as Ensemble EMD (EEMD) [7], Complementary EEMD (CEEMD) [8], and Complete EEMD with Adaptive Noise (CEEMDAN) [9] have been proposed to refine the decomposition performance. Nevertheless, those attempts to overcome the limitations of EMD do not fundamentally change the essence of EMD as a dyadic filter bank [10]. If the center frequencies of two oscillation modes are close enough, EMD will be incapable of generating desirable IMFs. Two or more oscillation modes sharing the same spectral band in the frequency domain of a single IMF is the so-called mode mixing phenomenon [1], which is inevitable when multiple modes are closely spaced with each other.

Efforts including adaptive filter [11], wavelet packet transform (WPT) [3], and frequency shifting [12] alleviate the mode mixing phenomenon in an ad hoc manner at the cost of the completeness and self-adaptability of EMD.

Variational mode decomposition (VMD) [13] is a newly developed signal decomposition technique well founded on a sound theoretical background and much more robust to sampling and noise. Contrary to EMD, VMD is an entirely nonrecursive algorism where modes are extracted concurrently. In particular, VMD searches for a given number of modes and their respective center frequencies adaptively. Each mode is band-limited around the center frequency which, to some extent, narrows the bandwidth of the extracted modes and eliminates the mode mixing phenomenon. Experiments have shown the superior performance of VMD with regard to tone detection, tone separation, and noise robustness compared to EMD [13].

In practical applications, however, the number of modes is required to be predefined. And the selection of the parameter that controls the tightness of the band limits is partially based on experience. Inappropriate combination of critical parameters will have predictable impact on the nature of detected modes. The suggestion proposed by the author in [13] is checking the spectral overlap or orthogonality between modes, or looking at the residuals.

Recent developments of the VMD method mainly concentrate on the field of fault diagnosis. With the assistance of the particle swarm optimization [14–16], multikernel support vector machine [17], the k-nearest neighbour algorithm [18], and other novel algorithms [19–21], promising results have been obtained. In a similar manner with the EMD denoising, the VMD has also been introduced to signal denoising based on the detrended fluctuation analysis [22, 23]. Moreover, the applicability of the VMD in identifying the electromechanical oscillatory modes has also been demonstrated in [24]. The identification process is based on the time-frequency analysis of nonlinear signals which arise after a large disturbance. The oscillatory power signal is converted into monocomponents through VMD and then the instantaneous modal characteristics are obtained via Hilbert transform.

Without loss of completeness, it is worthwhile to point out that, in addition to the aforementioned methods, other advanced decomposition techniques exist in the literature. Alternatively, the digital Taylor-Fourier transform (DTFT) could also be used to identify low-frequency electromechanical modes in power systems [25]. Instead of solving a variational problem in VMD, the DTFT decomposes a signal into monocomponents by spectral analysis using a filter bank. Some recent works related to chirp mode decomposition (CMD) are also concentrated on the signal decomposition. But the CMD and its improved versions mainly focus on the early fault detection and multifeature extraction of vibration signal with a fast fluctuating instantaneous frequency [26, 27]. Likewise, some time-frequency analysis methods [28–30] could also filter the target signal into desired monocomponents but with their own limitations.

Considering the modal parameter identification of a vibration system, however, the aforementioned successful applications may not be suitable. In addition, few researches on the selection of decomposition parameters that are applicable to the separation of modes and parameter identification have been found in the literature. Based on that concern, this paper emphasizes the accurate modal parameter identification taking advantage of the filter characteristics of the VMD algorithm.

The outline of this paper is as follows. Section 1 is the introduction. Section 2 introduces the primary mathematical principles of VMD and evaluates the filter performance when applied to fractional Gaussian noise (fGn). The predictable impact of the decomposition parameters on the nature of detected modes is also thoroughly investigated. Criteria for the selection of proper decomposition parameters that are applicable to the separation of modes and parameter identification of vibration system are established in Section 3. Section 4 extends the results to the ground vibration test (GVT) of a horizontal tail. Conclusions are listed in the last section.

2. VMD Analysis on fGn

2.1. Fractional Gaussian Noise. Fractional Gaussian noise (fGn) is defined as the increment process of fractional Brownian motion [31]. It is a zero-mean Gaussian stationary process whose autocorrelation sequence $r_H[k] := E\{x_H[n]x_H[n+k]\}$ reads

$$r_H[k] = \frac{\sigma^2}{2}\left(|k-1|^{2H} - 2|k|^{2H} + |k+1|^{2H}\right), \tag{1}$$

where k is a variable that denotes the time lag at which the autocorrelation is measured.

As is well known, the special case $H = 0.5$ reduces to white noise, whereas other values induce nonzero correlations, either negative if $0 < H < 0.5$ or positive if $0.5 < H < 1$. The description of fGn is mainly determined by the value of Hurst exponent, H, while the variance σ^2 is merely a scale parameter.

Taking the discrete Fourier transform of equation (1), the power spectrum density of fGn is obtained:

$$S_H(f) = C\sigma^2\left|e^{i2\pi f} - 1\right| \sum_{k=-\infty}^{\infty} \frac{1}{|f+k|^{2H+1}}, \tag{2}$$

with $|f| \le 0.5$. If $H \neq 0.5$, then $S_H(f) \sim C\sigma^2|f|^{1-2H}$ when f approaches zero. It, therefore, follows that fGn is a convenient model for power-law spectrum at low frequencies [32]. If $0 < H < 0.5$, the spectrum is high-pass having $S_H(0) = 0$. On the other hand, if $0.5 < H < 1$, a "$1/f$"-type spectral divergence is delineated with $S_H(0) = \infty$.

2.2. Brief Review of VMD. The goal of VMD is to decompose a real-valued input signal f into a given number of modes $\{u_k\}$ and each is assumed to be mostly compact around a center pulsation $\{\omega_k\}$. The definition of mode u_k in VMD is an amplitude-modulated-frequency-modulated (AM-FM) signal, written as

$$u_k(t) = A_k(t)\cos\left(\varphi_k(t)\right), \tag{3}$$

which is more mathematically rigorous than the so-called IMF. The search for $\{u_k\}$ and $\{\omega_k\}$ results in a constrained variational problem as follows:

$$\min_{\{u_k\},\{\omega_k\}} \quad \left\{ \sum_k \left\| \partial_t \left[\left(\delta(t) + \frac{j}{\pi t} \right) u_k(t) \right] e^{-j\omega_k t} \right\|_2^2 \right\}, \qquad \text{s.t.} \quad \sum_k u_k = f, \tag{4}$$

where $\{u_k\} := \{u_1, \ldots, u_k\}$ and $\{\omega_k\} := \{\omega_1, \ldots, \omega_k\}$ are shorthand notations for the set of all modes and their center frequencies, respectively. In order to render the problem unconstrained, both a quadratic penalty and Lagrangian multipliers λ are used. The augmented Lagrangian L is introduced as

$$L(\{u_k\},\{\omega_k\},\lambda) = \alpha \sum_k \left\| \partial_t \left[\left(\delta(t) + \frac{j}{\pi t} \right) u_k(t) \right] e^{-j\omega_k t} \right\|_2^2 + \left\| f(t) - \sum_k u_k(t) \right\|_2^2 + \langle \lambda(t), f(t) - \sum_k u_k(t) \rangle, \tag{5}$$

where α denotes the constraint parameter of the data fidelity that controls the tightness of the band limits. The saddle point of the augmented Lagrangian L is the solution to the original minimization problem of equation (4). Detailed implementation can be found in [13]. Particularly, the modes are updated by simple Wiener filtering directly in Fourier domain which makes the algorism more robust to sampling and noise.

2.3. Filter Performance of VMD on fGn. Similar to some previous studies [10, 32, 33], extensive simulations are carried out on fGn processes with H being set to three typical values 0.2, 0.5, and 0.8, and the variance σ^2 being fixed to 1 for all samples. The data length is taken to be $N = 1024$ and, for each value of H, 1000 independent sample paths of fGn are generated via the Wood and Chan algorithm [34]. Given the data sets, the VMD is realized for all sample paths resulting in a collection of modes. Spectral analysis is carried out for each mode of each realization. The Fourier spectra of each mode u_k are averaged and arranged mode by mode in Figure 1. The number of modes K is set to 5 with uniformly distributed initial center frequencies. That is, $\{\omega_k^1\} = \{0, 0.1, 0.2, 0.3, \text{ and } 0.4\,\text{Hz}\}$.

For comparison purposes, the averaged Fourier spectra of IMFs for EMD realizations are also displayed in Figure 2. As evidenced in Figures 1 and 2, the collection of the extracted modes $\{u_k\}$ by VMD tends to self-organize in a filter bank structure which is similar to what is classically observed in wavelet packet decomposition rather than the wavelet-like structure exhibited in EMD [32]. Practically, all the extracted modes $\{u_k\}$ are equivalent band-pass filters, which are different from EMD where the filter associated with the 1st mode is essentially high-pass. The spectral band of the analyzed sample paths of fGn is divided into five discrete subfrequency regions almost evenly. That is to say, the bandwidth of each filter is practically identical to each other evolving with the uniformly distributed predominant center frequencies. Moreover, the increase of constraint parameter α narrows the pass-band of each filter and thus minimizes the overlap between the separated modes simultaneously.

In a detailed investigation, the averaged center frequencies and the energy distribution of the extracted five modes are calculated and plotted against the modal order in Figures 3 and 4, respectively. Regardless of the value of α, the energy distribution shown in Figure 4 successfully characterizes the power spectrum density of fGn. As mentioned in the previous subsection, in the case of $H = 0.2$, the spectrum is high-pass and, therefore, follows an increasing trend of energy proportion versus the modal order; while in the case of $H = 0.8$, the "$1/f$"-type spectral divergence is captured; for the special case of $H = 0.5$, the power spectrum density is a constant which is also true for the energy distribution. The impact of the constraint parameter α on the center frequencies $\{\omega_k\}$ may not be convincing as depicted in Figure 3, yet it still drops some results. The center frequencies $\{\omega_k\}$ skewed either to the right or left characterizing the spectrum of fGn for a small value of α are forced to converge to the uniformly initialized center frequencies $\{\omega_k^1\}$ with the increase of α.

2.4. Impact of Initialization and Constraint Parameter α on Filter Performance. In order to further verify the impact of constraint parameter α on the convergence, the normalized center frequencies are initialized randomly as

$$\left\{ \frac{\omega_k^1 \mid \omega_k^1 = N^{\varepsilon_k - 1}}{2^{\varepsilon_k}, \varepsilon_k \sim U(0,1)}, \quad k = 1, \ldots, K \right\}, \tag{6}$$

where N is the data length which is 1024 in all simulations of this paper. Statistically, the base-2 logarithm of the initial center frequencies is uniformly distributed, as shown in Figure 5, whereas the regular values are concentrated in the low-frequency band.

Distinguished from the results obtained where the center frequencies are initialized uniformly, the averaged Fourier spectra, as illustrated in Figure 6, tend to organize in disorder with merely no statistical law to find, in the case of a larger value of α. Whereas the filter bank structures observed in the case of $\alpha = 1e3$ coincide with those generated in the previous realizations as the dashed lines depicted in Figure 6 overlap with the blue ones except for the case of $H = 0.8$. Scatter diagrams of the initial center frequencies $\{\omega_k^1\}$ versus the converged center frequencies $\{\omega_k^n\}$ as shown in Figure 7, where each mode is denoted by a corresponding color, demonstrate a growing linear relationship between each other with the increase of α. Linear stripe patterns that are distinct from each other are visible in Figure 7(a), indicating that the adaptability is successfully recovered regardless of the initialization in the case of a small value of α. Moreover, the histograms plotted in Figure 8 also suggest the same result since the empirical probability density distribution of the converged center frequencies $\{\omega_k^n\}$ gradually evolves to that of the $\{\omega_k^1\}$, with an increasing value of α. While only the

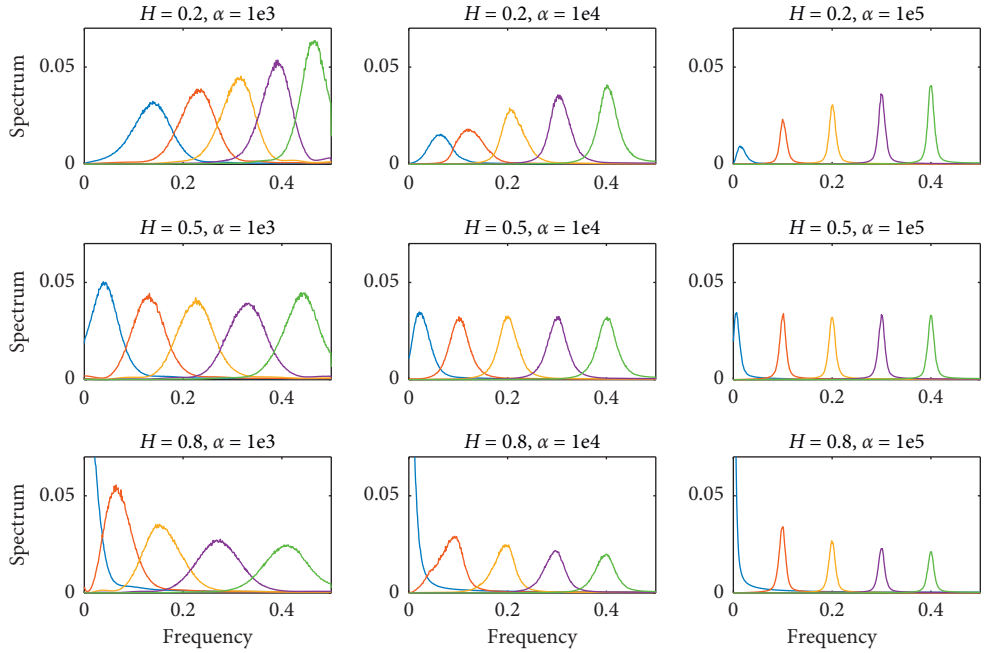

FIGURE 1: The averaged Fourier spectra of extracted modes $\{u_k\}$ for VMD realizations, in the case of three typical Hurst exponents: $H = 0.2$ (1st row), $H = 0.5$ (2nd row), and $H = 0.8$ (3rd row). The initial center frequencies $\{\omega_k^1\}$ were uniformly distributed, for three different values of α (α = 1e3 (1st column), 1e4 (2nd column), and 1e5 (3rd column)).

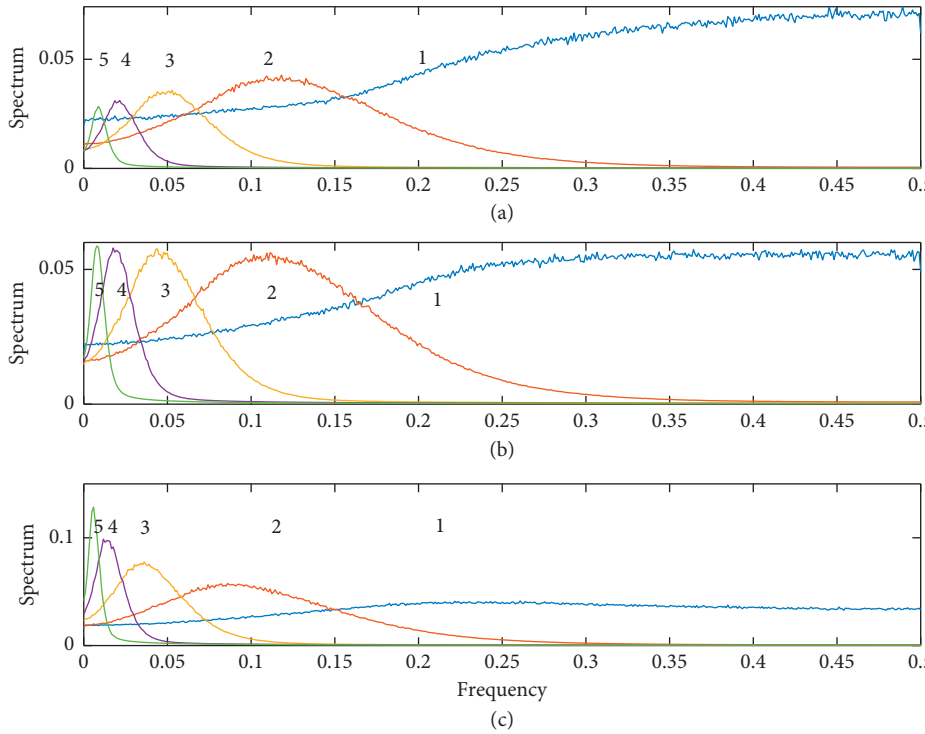

FIGURE 2: The averaged Fourier spectra of IMFs for EMD realizations, in the case of three typical Hurst exponents: (a) $H = 0.2$, (b) $H = 0.5$, and (c) $H = 0.8$.

convergence analysis in the case $H = 0.2$ is demonstrated here, the same results could be observed regardless of the Hurst exponent.

In summary, the filter performance of VMD does depend on the initialization as well as the value of constraint parameter α, suggesting that the algorithm does not

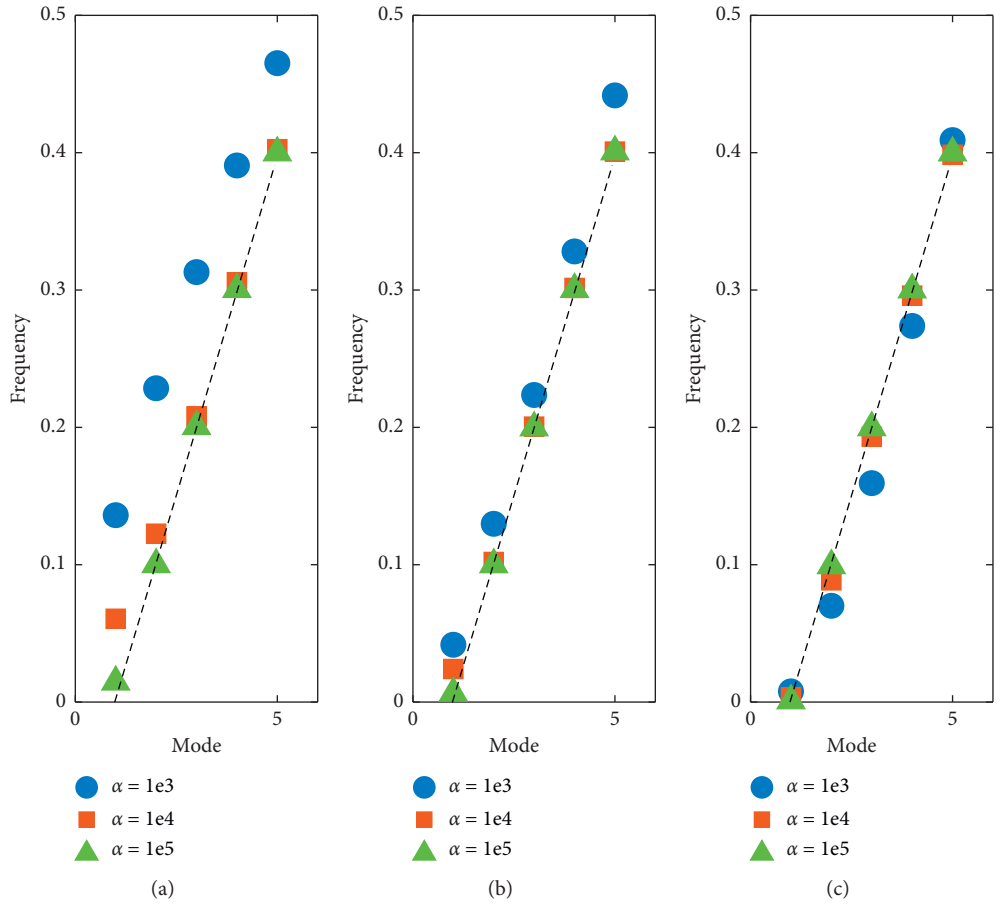

FIGURE 3: The averaged center frequencies $\{\omega_k^n\}$ of each mode u_k, in the case of three typical Hurst exponents: (a) $H = 0.2$, (b) $H = 0.5$, and (c) $H = 0.8$. The dashed lines denote the uniformly initialized center frequencies plotted as a function of modal order.

necessarily converge to a global minimum. From a different point of view, the selection of α and initial center frequencies $\{\omega_k^1\}$ could be refined to extract a collection of desired modes.

3. Separation of Modes Based on VMD

3.1. Parameter-Optimized VMD. Inspired by the conclusion of the previous section, criteria for the optimization of α and the initialization of center frequencies $\{\omega_k^1\}$ are proposed in this section, in order to extract a collection of desired modes of vibration system. For an actual dynamic structure containing closely spaced modes, the identification of modal frequency is much more efficient and accurate than the damping ratio, since each significant peak in frequency domain could be roughly taken as one natural mode. Hence, the predominant center frequencies of the equivalent band-pass filters in VMD realization are to be initialized by the prior identified modal frequencies utilizing the simple peak-picking method and there follows the number of modes K. However, the desired value of α must be able to separate the coupled spectrum of closely spaced modes and retain the most modal information simultaneously. The strategy suggested here is optimizing the value of α through genetic algorithm (GA). The constructed fitness function is described as

$$\text{fitness} = \left(1 - \sum_{k=1}^{K} \frac{\int u(t)_k^2 \mathrm{d}t}{\int f(t)^2 \mathrm{d}t}\right)\left(1 - \min\{r(u_k, f), k = 1, \ldots, K\}\right) + \varepsilon, \tag{7}$$

where $r(u_k, f)$ denotes the correlation coefficient between a mode u_k, f and the analyzed signal f; ε denotes the penalty factor that is taken as the number of duplicate modes by checking the matrix of correlation coefficients for the extracted modes $\{u_k\}$. Duplicate modes are detected when the correlation coefficient $r(u_i, u_j)$ between two separated modes is extremely large. The optimal value of α_{opt} satisfies $\alpha_{\text{opt}} = \text{argmin}_\alpha(\text{fitness})$. The instantaneous modal information of each monocomponent subsignal u_k thus can be derived through the Hilbert transform. Primary steps of the parameter-optimized VMD realization are as follows:

Step 1. Preestimate the modal frequencies $\{\omega_i, i = 1, 2, \ldots, M\}$ of the analyzed signal f using simple peak-picking method.

Step 2. Initialize the center frequencies $\{\omega_k^1\} = \{\omega_i\}$ and there follows the number of modes $K = M$.

Step 3. Search for the optimal value $\alpha_{\text{opt}} = \text{argmin}_\alpha(\text{fitness})$ through GA.

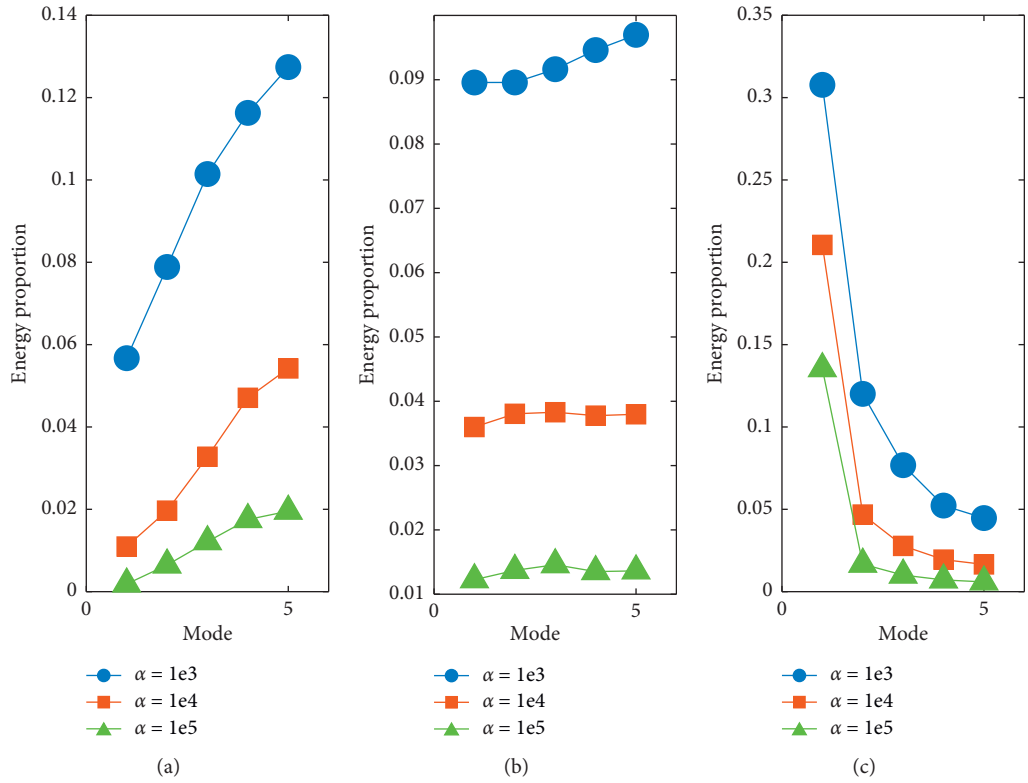

Figure 4: The averaged energy proportion of each mode u_k plotted as a function of modal order, in the case of three typical Hurst exponents: (a) $H = 0.2$, (b) $H = 0.5$, and (c) $H = 0.8$.

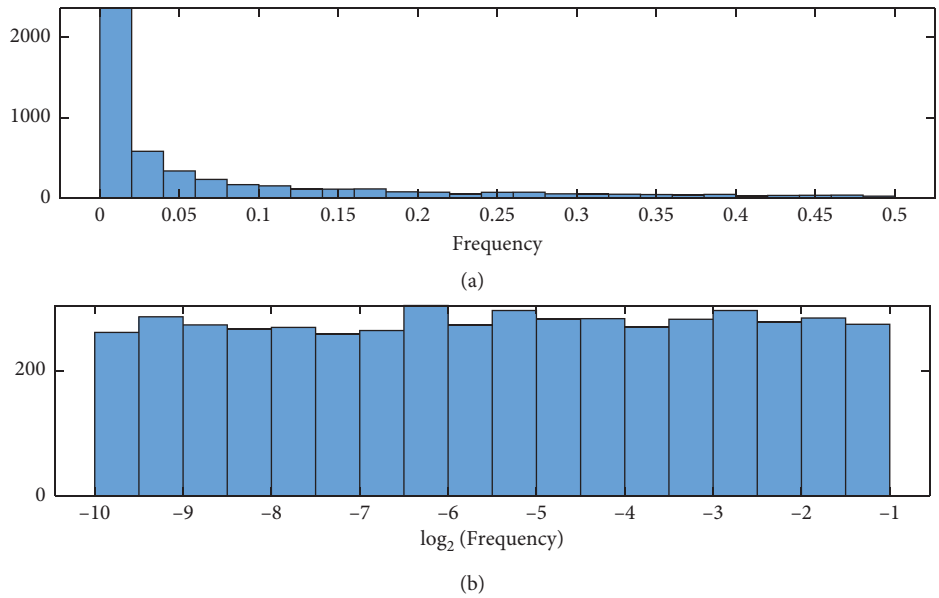

Figure 5: (a) Histogram of the randomly initialized center frequencies $\{\omega_k^1\}$; (b) histogram of the base-2 logarithm of the randomly initialized center frequencies $\{\log_2(\omega_k^1)\}$.

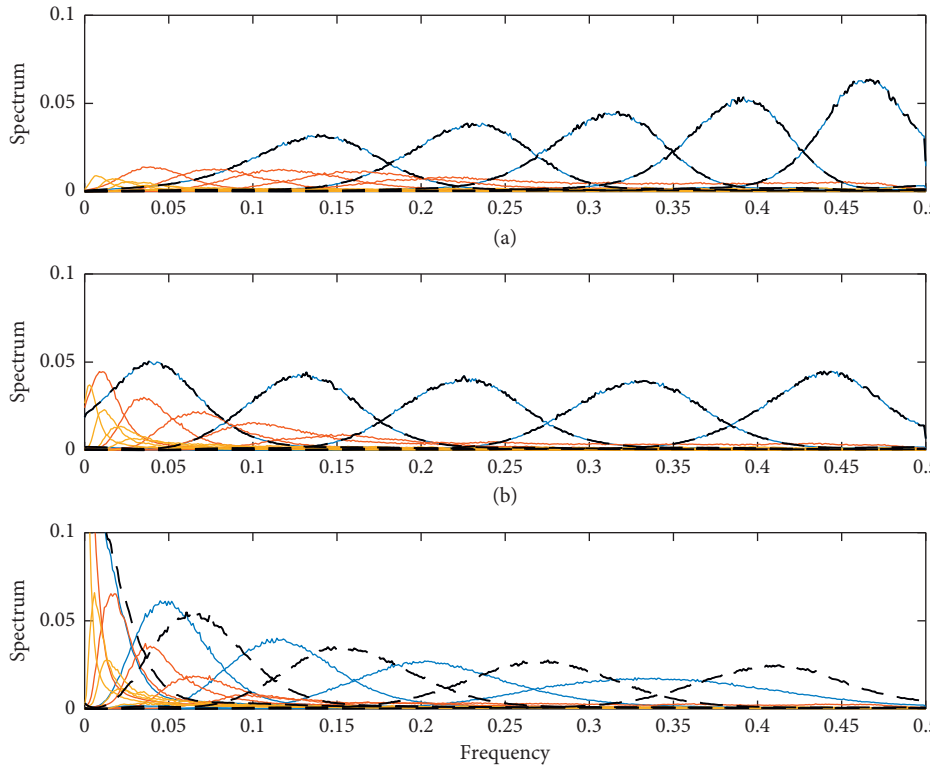

FIGURE 6: The averaged Fourier spectra of extracted modes $\{u_k\}$ for VMD realizations, in the case of three typical Hurst exponents: (a) $H = 0.2$, (b) $H = 0.5$, and (c) $H = 0.8$. The center frequencies $\{\omega_k^1\}$ were initialized randomly, for three different values of α ($\alpha = 1e3$ (blue lines), 1e4 (red lines), and 1e5 (yellow lines)). The dashed lines denote the averaged spectra illustrated in Figure 1 in the case of $\alpha = 1e3$.

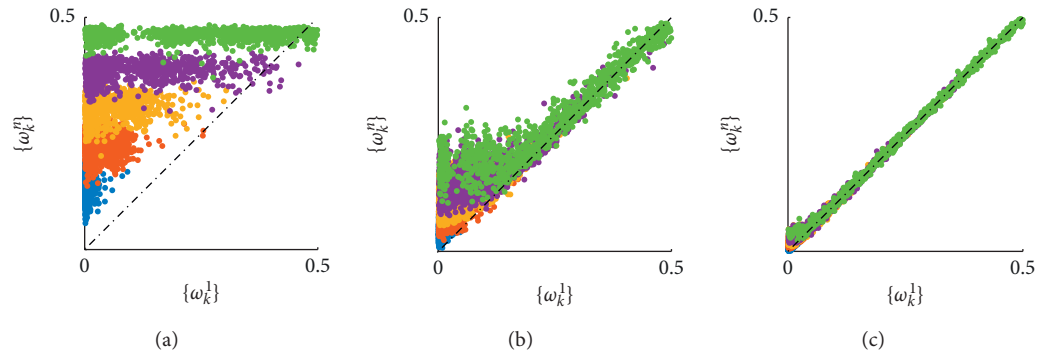

FIGURE 7: Scatter plots of initial center frequencies $\{\omega_k^1\}$ versus the converged center frequencies $\{\omega_k^n\}$, in the case of three different values of constraint parameter (a) $\alpha = 1e3$, (b) $\alpha = 1e4$, and (c) $\alpha = 1e5$, where the Hurst exponent $H = 0.2$.

Step 4. Decompose the signal f into a desired number of modes $\{u_k\}$ with the parameter-optimized VMD.

Step 5. Derive the analytic signal $u_{k,A}$ of each mode by Hilbert transform and obtain $u_{k,A}(t) = A_k(t)e^{j\phi(t)}$. Supposing the signal f is the impulse response of a small damping vibration system, we have $\omega(t) = d\phi(t)/dt = \omega_k\sqrt{1-\zeta_k^2}$ and $\ln A_k(t) = -\zeta_k\omega_k t + c$. Thus, the modal frequency ω_k and damping ratio ζ_k are identified by least squares method.

3.2. Numerical Experiment. A 2-dof parametric system as shown in Figure 9 is designed to evaluate the performance of the proposed method on the separation of modes. The dynamics of the system are described by equation (8):

$$\begin{bmatrix} m & 0 \\ 0 & m \end{bmatrix}\begin{bmatrix} \ddot{u}_1 \\ \ddot{u}_2 \end{bmatrix} + \begin{bmatrix} c_1 + c_2 & -c_2 \\ -c_2 & c_2 + c_3 \end{bmatrix}\begin{bmatrix} \dot{u}_1 \\ \dot{u}_2 \end{bmatrix} + \begin{bmatrix} (1+\mu)k & -\mu k \\ -\mu k & (1+\mu)k \end{bmatrix}\begin{bmatrix} u_1 \\ u_2 \end{bmatrix} = \begin{bmatrix} \delta(t) \\ 0 \end{bmatrix}, \tag{8}$$

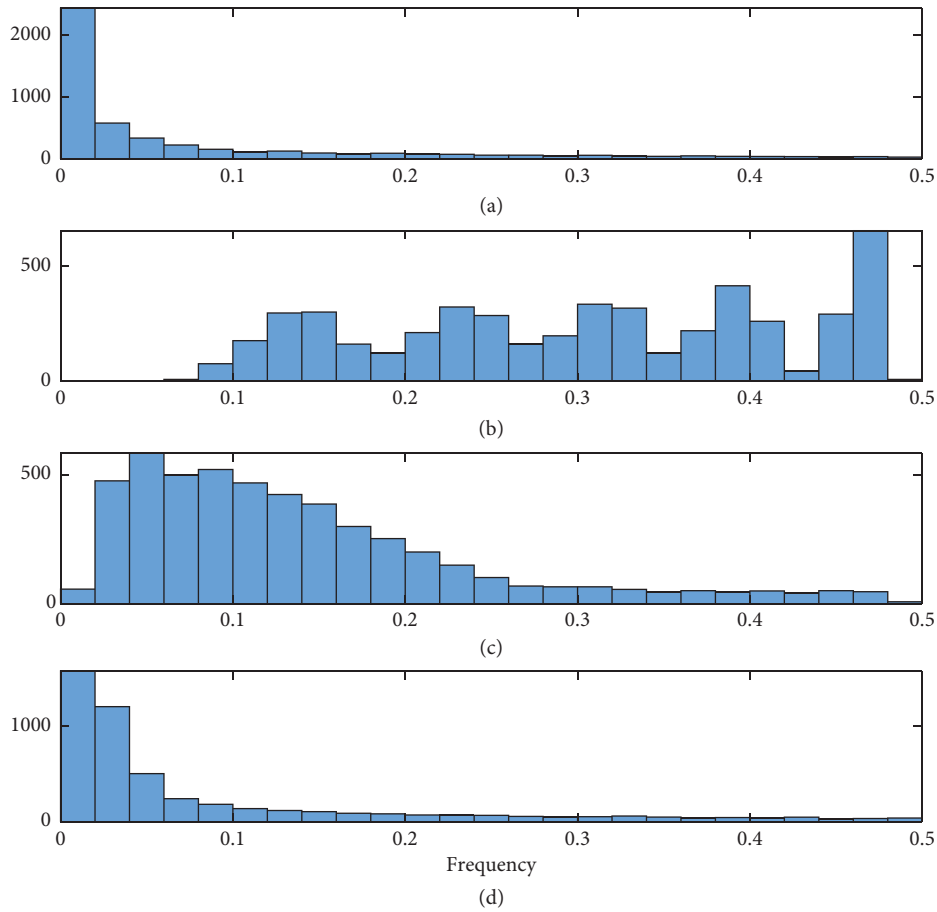

Figure 8: (a) Histogram of the randomly initialized center frequencies $\{\omega_k^1\}$ and the converged center frequencies $\{\omega_k^n\}$, in the case of three different values of constraint parameter (b) $\alpha = 1e3$, (c) $\alpha = 1e4$, and (d) $\alpha = 1e5$, where the Hurst exponent $H = 0.2$.

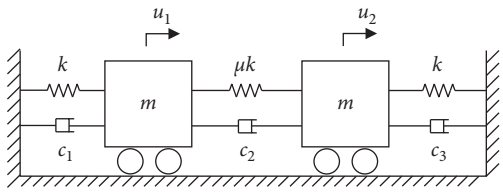

Figure 9: 2D of parametric system.

where the $\delta(t)$ is the impulsive load. The two natural frequencies derived are

$$\omega_1 = \sqrt{\frac{k}{m}},$$
$$\omega_2 = \sqrt{(1+2\mu)\frac{k}{m}} = \omega_1\sqrt{1+2\mu}, \tag{9}$$
$$\gamma \triangleq \frac{\omega_1}{\omega_2 = 1/\sqrt{1+2\mu}} \in (0,1). \tag{10}$$

By changing the value of μ, the ratio γ of the two natural frequencies is altered. Given the designed values of damping ratio (ζ_1, ζ_2), the damping matrix $\mathbf{C}$ is reconstructed as

$$\mathbf{C} = a\mathbf{M} + b\mathbf{K},$$
$$\begin{pmatrix} a \\ b \end{pmatrix} = \frac{2\omega_1\omega_2}{\omega_2^2 - \omega_1^2}\begin{bmatrix} \omega_2 & -\omega_1 \\ \dfrac{1}{\omega_2} & \dfrac{1}{\omega_1} \end{bmatrix}\begin{pmatrix} \zeta_1 \\ \zeta_2 \end{pmatrix}, \tag{11}$$

where $\mathbf{M}$ denotes the mass matrix and $\mathbf{K}$ denotes the stiffness matrix.

In the present numerical experiment, the displacement response u_2 is recorded as the output signal with a sampling frequency $F_s = 1024$ Hz. The structural parameters are chosen with $m = 1$ kg, $k = 8000$ N/m, $\gamma = 0.8$, $\zeta_1 = 0.01$, and $\zeta_2 = 0.015$. Besides, an additional zero-mean Gaussian white noise is added to the output response simulating the measurement noise. The signal-to-noise ratio (SNR) is set to 20 dB.

The EEMD and CEEMDAN are realized on the contaminated response signal. Eliminating the first two IMFs containing high-frequency noise and the last several trends, the primary modes are plotted in Figures 10 and 11, respectively. The results are unsatisfying because both realizations not only fail to separate the two oscillation modes but also generate additional pseudocomponents. Contrary to the noise-assisted versions of EMD realizations, the wavelet

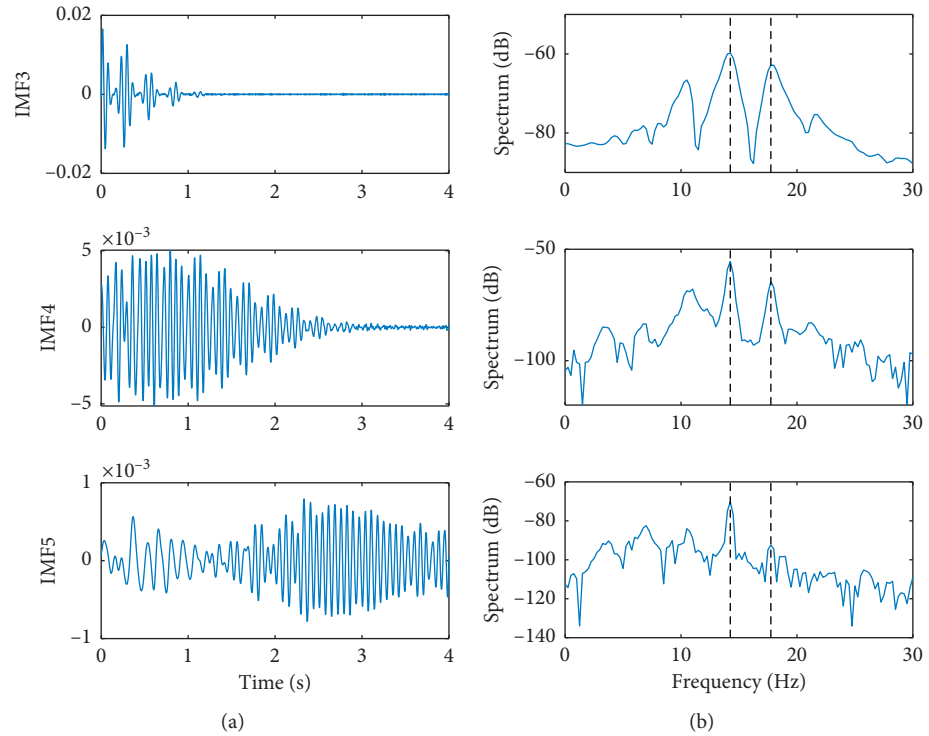

Figure 10: (a) The extracted three modes by EEMD and (b) the corresponding Fourier spectra.

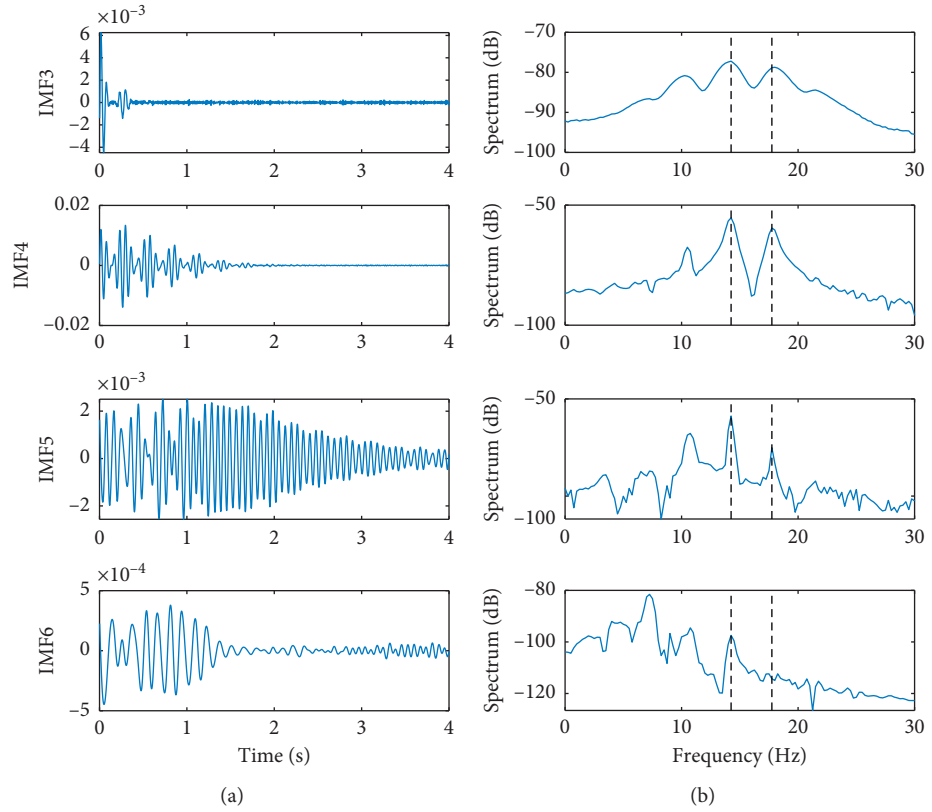

Figure 11: (a) The extracted four modes by CEEMDAN and (b) the corresponding Fourier spectra.

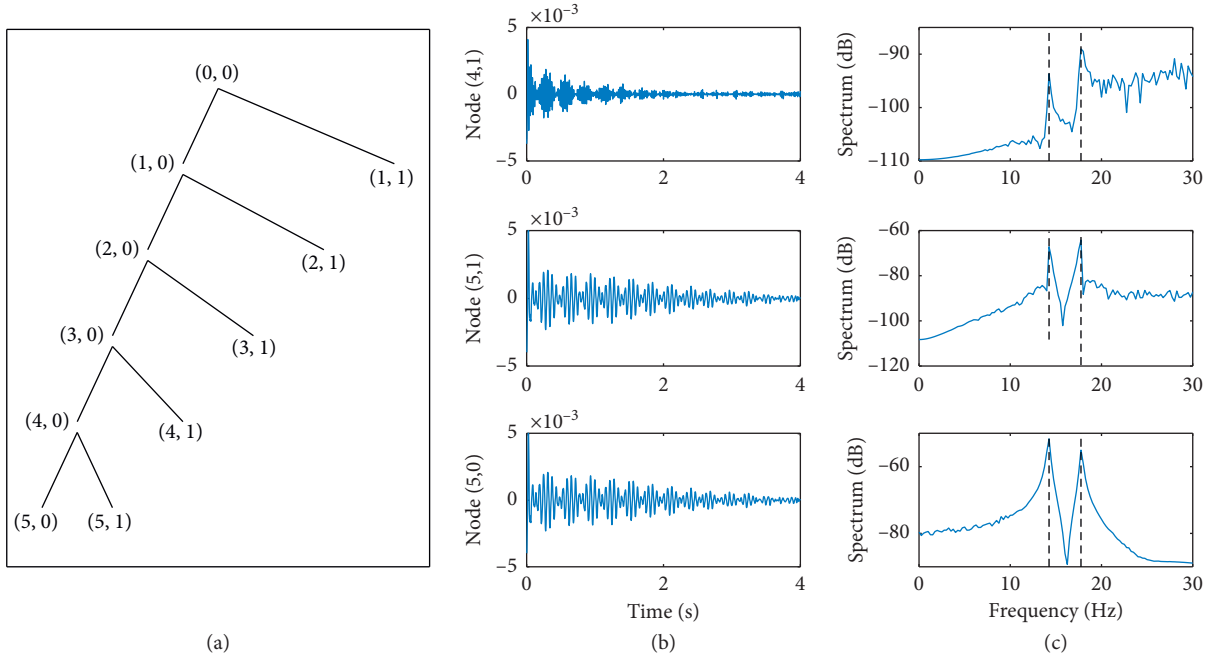

FIGURE 12: Results of the wavelet packet transform. (a) The optimized best decomposition tree. (b) Reconstruction data on nodes (4, 1), (5, 1), and (5, 0), with (c) their corresponding Fourier spectra.

packet transform (WPT) identifies the situation as a single AM-modulated signal as evidenced in Figures 12(b) and 12(c). The best tree is shown in Figure 12(a) corresponding to the decomposition result down to level 5 using the db4 wavelet. In this case, the best tree reduces to the wavelet tree, and the WPT merely plays the role of signal denoising.

Different from the failed attempts to decompose the signal into separate monocomponents, the proposed parameter-optimized VMD successfully captures the two oscillation modes. As illustrated in Figure 13(b), although there is a slight mixture of modal contribution considering the relative amplitude, the decomposed results obtained by the optimized VMD outperform the implementation of EEMD, CEEMDAN, and WPT. The desired two oscillation modes are extracted concurrently while preserving the dynamics of the signal. Both resonances and antiresonances remain at the same frequency lines, which is not the case of the obtained using WPT in Figure 12; even this appears to be the smoother and better reconstructed spectra. The PolyMAX identification results in Figure 14, which will be discussed later, further support the argument since the antiresonance is present, apparently at the same frequency line as identified by the two extracted modes in Figure 13. Compared with the theoretical time history of the desired modes in Figure 13(a), the error is mainly concentrated on the left boundary due to the simple mirror extension of the signal as suggested in [13]. The boundary issues are also classically observed in EMD which could be only partially alleviated by more mathematically attempts. Furthermore, the obtained Hilbert spectrum as shown in Figure 13(c) manages to reflect the true frequency pattern of the inspected signal. The identified modal frequencies are $f_1 = 14.23$ Hz and $f_2 = 17.81$ Hz with the percentage error of 0.01% and 0.1%, respectively. The damping ratios are $\zeta_1 = 1.01\%$ and $\zeta_2 = 1.47\%$ with the percentage error of 1.42% and 2.31%. For comparison purpose, traditional modal parameter identification is conducted utilizing the PolyMAX method in frequency domain with the aid of stabilization diagram [35]. The results are illustrated in Figure 14. The identified modal frequencies are $f_1 = 14.29$ Hz and $f_2 = 17.83$ Hz with the percentage error of 0.38% and 0.18%. The damping ratios, however, are $\zeta_1 = 2.00\%$ and $\zeta_2 = 2.97\%$ with the considerable percentage error of 100.42% and 97.81%.

Compared with some other adaptive signal decomposition methods and the modal parameter identification using PolyMAX in frequency domain, the proposed parameter-optimized VMD is superior in separating closely spaced modes and retaining the most modal information simultaneously. While only the case $\gamma = 0.8$ at the noise level of SNR = 20 dB is displayed in this section, more complete numerical experiments within the range $0.5 \leq \gamma \leq 0.9$ under the noise condition of SNR = 20 dB and 10 dB are carried out. The identified modal parameters are listed in Table 1. It appears that the identification of modal frequency is much more accurate than the damping ratio. Despite that, the maximum percentage error of damping identification is still within 5% which is acceptable in engineering practice. The complete investigation further demonstrates the effectiveness of the presented method based on VMD in separating closely spaced modes of vibration system.

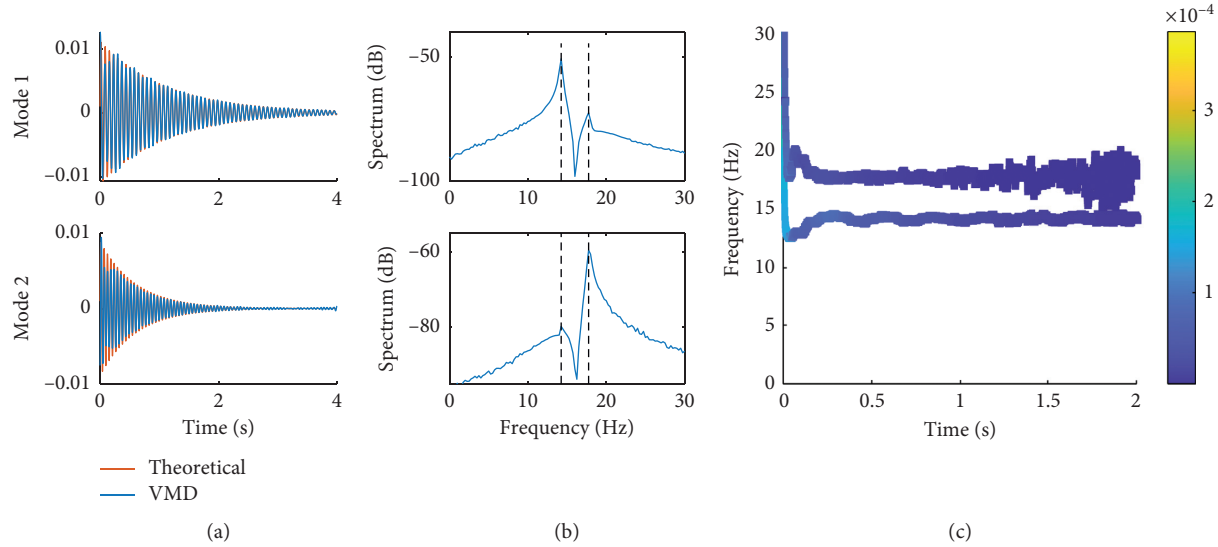

Figure 13: (a) The two separated modes by the proposed method with (b) the corresponding Fourier spectra and (c) the Hilbert spectrum.

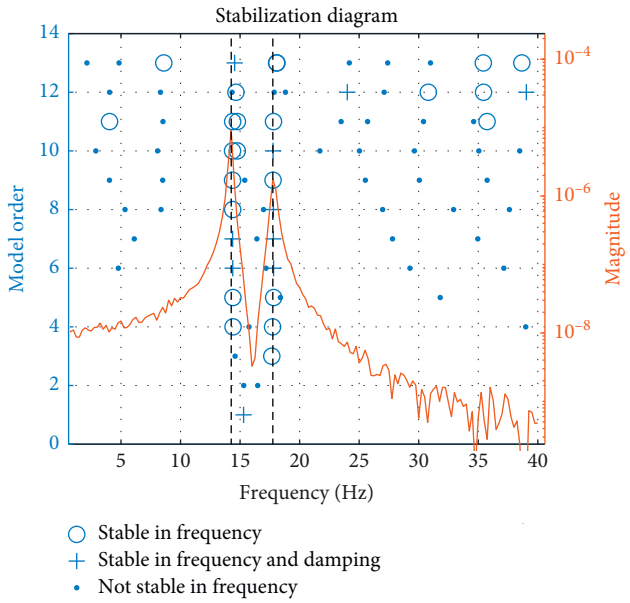

Figure 14: Stabilization diagram utilizing PolyMAX identification in frequency domain.

3.3. Computational Complexity. The computational complexity of a VMD algorithm depends on the initialization of the center frequency of each mode and the recursive Fast Fourier Transform (FFT). As is well known, the computational complexity of the FFT algorithm is O ($N \log N$), where N is the length of the transform domain signal or the number of points in DFT. For the extraction of the k number of modes, the computational complexity of the VMD realization will be the sum of the required computations for the initialization of center frequencies and k O($N \log N$) [24]. Besides, the presented optimized version of VMD adds an extra requirement, which increases the computational cost and it is also subjective, in terms of which optimization technique should be deployed, not to mention its specific parametrization.

Table 2 shows the comparison of the computational cost of the presented decomposition techniques. The computational complexity of the EMD/EEMD has proven to be equivalent to that of the FFT but with a larger factor [36]. As an improved version of EEMD, the CEEMDAN algorithm does not fundamentally change the core structure of EEMD but improves the procedure of the noise-enhanced realization of EMD [9]. Therefore, in terms of computational complexity, the presented versions of EMD along with WPT are identical to each other. It should be noted that the specific computational complexity of VMD has not been found in the literature and will not be given in this paper, which is beyond the scope of this research. Despite that, the complexity of the VMD algorithm exceeds that of the presented decomposition techniques, not to mention the optimized version.

A numerical experiment is performed to verify the actual computational cost of the decomposition techniques including the original VMD algorithm and the optimized version. The experiment is conducted on a laptop computer with 2.6 GHz CPU and 8 GB memory under the MATLAB environment. The simulation is repeated 100 times for each decomposition technique and the average execution time for each implementation is obtained. The test signal is the displacement response of the 2-dof parametric system recorded at the sampling rate of 1024 Hz and the ratio of the two natural frequencies γ set to 0.8, which is the same as that demonstrated in the previous section. Moreover, the specific parameter settings are consistent with those demonstrated in the previous section to obtain the same results as illustrated in Figures 10–13.

As shown in Table 2, without considering the decomposition results, the EMD and WPT are both computationally efficient. The execution time of EEMD and CEEMDAN, however, differs greatly with that of EMD, which is because both algorithms require extensive noise-enhanced realizations of EMD to alleviate the mode mixing phenomenon [7–9]. When it comes to each realization, the

Table 1: The identified modal parameters.

γ	Order	SNR = 20 dB				SNR = 10 dB			
		f (Hz)	Error (%)	ζ (%)	Error (%)	f (Hz)	Error (%)	ζ (%)	Error (%)
0.5	1	14.24	0.02	1.01	0.97	14.24	0.05	1.02	2.12
	2	28.50	0.09	1.49	0.69	28.45	0.07	1.50	0.23
0.6	1	14.23	0.01	1.00	0.44	14.23	0.02	1.04	3.91
	2	23.72	0.01	1.47	2.07	23.74	0.06	1.54	2.67
0.7	1	14.24	0.02	1.00	0.09	14.23	0.02	0.98	2.04
	2	20.34	0.02	1.51	0.63	20.35	0.05	1.48	1.21
0.8	1	14.23	0.01	1.01	1.42	14.23	0.02	0.96	3.58
	2	17.81	0.10	1.47	2.31	17.82	0.13	1.44	3.89
0.9	1	14.25	0.10	1.02	2.43	14.24	0.00	1.05	4.56
	2	15.81	0.04	1.54	2.86	15.82	0.03	1.45	3.26

f denotes the modal frequency and ζ denotes the damping ratio.

Table 2: The computational cost of the presented decomposition techniques.

Decomposition technique	Computational complexity	Execution time (s) ($N = 4096$)
EMD	O ($N \log N$)	0.031
EEMD	O ($N \log N$)	32.086 (NR = 800)
CEEMDAN	O ($N \log N$)	7.170 (NR = 80)
WPT	O ($N \log N$)	0.030 (db4, level 5)
VMD (original)	—	0.180 ($\alpha = 2000$, $K = 2$)
VMD (optimized)	—	84.514

N is the data length and NR denotes the number of realizations.

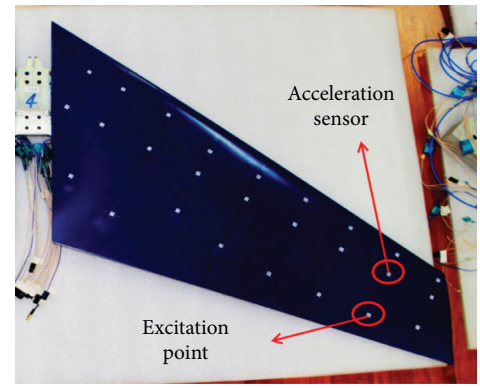

Figure 15: Test horizontal tail.

average execution time of each noise-enhanced EMD realization for EEMD is 0.040 s while it takes 0.090 s on average to realize a noise-enhanced EMD implementation for CEEMDAN. Thus, if we do not consider the influence of the parameter NR on the increase of execution time, the computational cost of the first four decomposition techniques listed in Table 2 is also the same in terms of the order of magnitude. Relatively, the execution time of the original VMD implementation is increased by one order of magnitude, where the parameter α is arbitrarily taken as $\alpha = 2000$. While only the case $\alpha = 2000$ is demonstrated in this section for the sake of readability, in a more complete experiment, the value of α has little impact on the execution time when the number of modes is fixed to $K = 2$. Compared with the original VMD implementation, the presented optimized version increases the computational cost by two orders of magnitude. This means that after hundreds of VMD realizations, the optimal parameter could be finally determined, which is inevitable no matter what optimization technique should be deployed, because, basically, the optimization is the process of trial and error. Although the presented optimized VMD consumes much more time than other decomposition techniques, the decomposition results of the optimized VMD outperform the compared techniques in the separation of closely spaced modes while preserving the most modal information at the same time. Since the priority of modal analysis is the accuracy of the identified modal parameters, the additional computational cost of the presented optimized VMD could be tolerant in practical applications, whereas the compared methods lose their validity in the same situation.

3.4. Ground Vibration Test of a Horizontal Tail. Ground vibration test (GVT) of a horizontal tail using a hammering method is conducted to analyze the dynamic characteristics of the structure. The test horizontal tail as pictured in Figure 15 consists of a metal beam and composite frames that provide the airfoil shape. The wing structure was manufactured by 3D printing and covered with composite skin. In order to check the vertical bending and torsion modes, the acceleration sensor was fixed at a selected point while the hammer excited the structure at different locations to estimate the frequency response functions (FRFs). The test data obtained in the case of the distribution of acceleration sensor and excitation point as illustrated in Figure 15 is adopted to verify the effectiveness of the proposed method based on VMD. The sampling frequency of the test data is 1024 Hz with a 5-second duration.

The Fourier spectrum, or rather FRF, of the response signal is shown in Figure 16(b) where only the first five modes are considered here. A low-pass filter with the pass-band frequency of 80 Hz is designed to remove the high-frequency response. The selection of the filter band is a manual process. The modal frequencies of the five natural modes are arbitrarily estimated by the peak-picking method

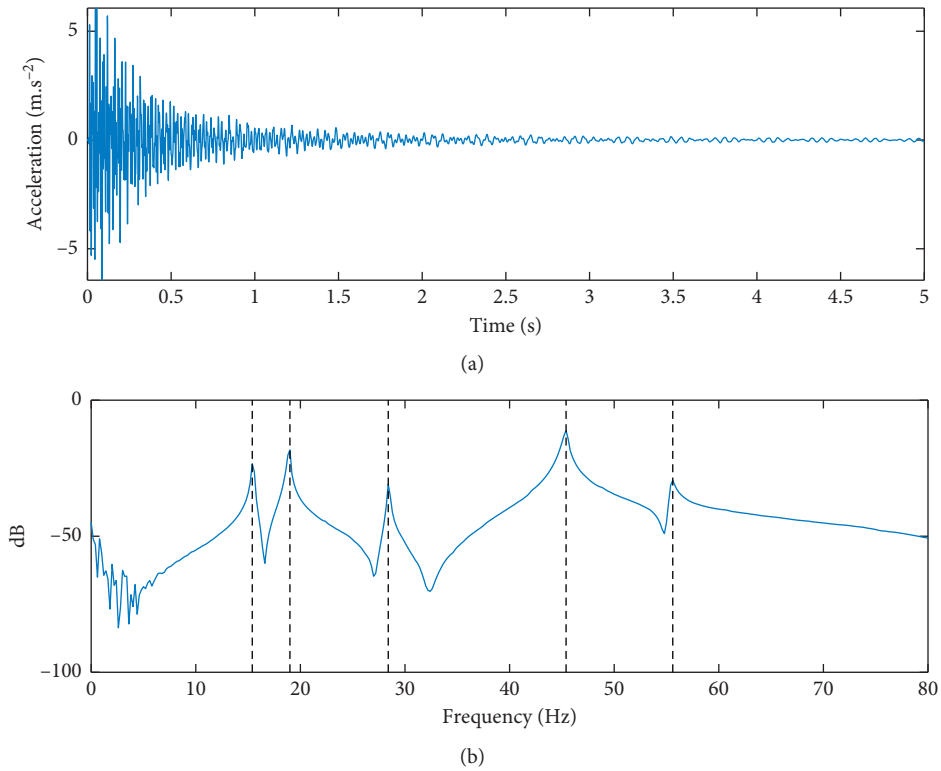

Figure 16: (a) Time history of the wingtip acceleration response and (b) its Fourier spectrum.

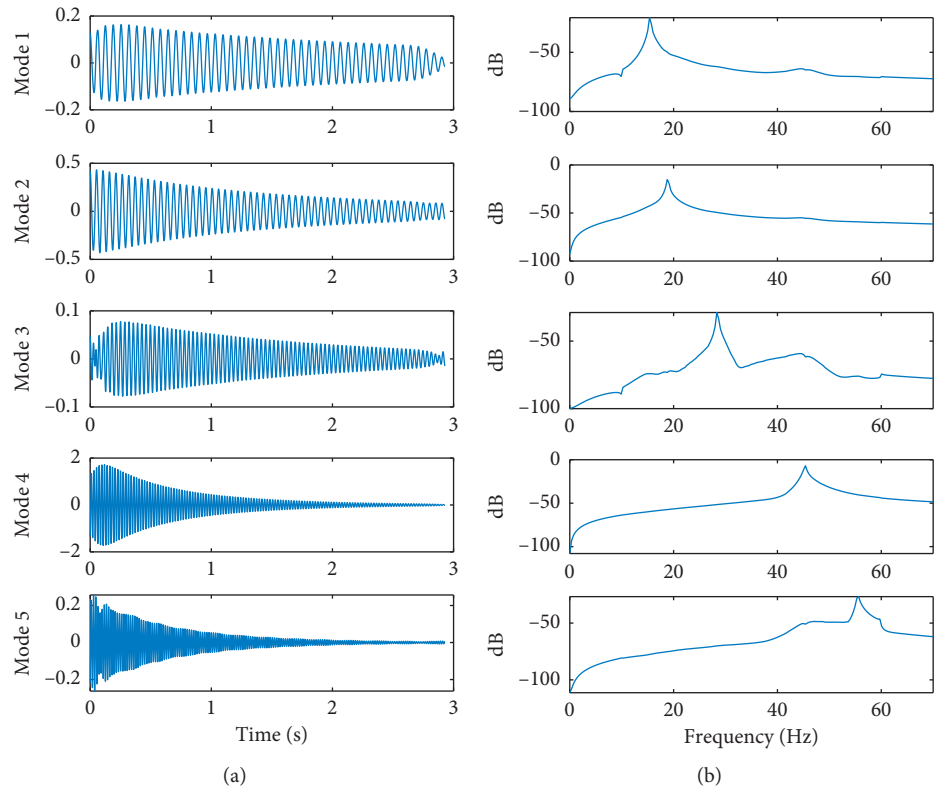

Figure 17: (a) The extracted five modes by the proposed method based on VMD and (b) the corresponding Fourier spectra.

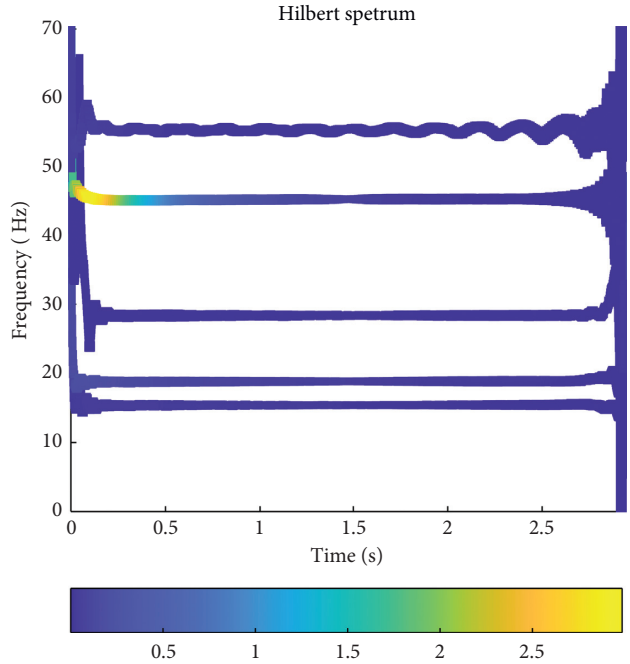

Figure 18: Hilbert spectrum of the extracted five modes.

Table 3: The identified modal parameters.

	Order	Theoretical values	PolyMAX in the frequency domain	Error (%)	Proposed method based on VMD	Error (%)
f (Hz)	1	15.507	15.487	0.129	15.482	0.159
	2	18.941	18.916	0.135	18.911	0.159
	3	28.513	28.511	0.007	28.496	0.059
	4	45.526	45.431	0.012	45.452	0.162
	5	55.646	55.659	0.023	55.639	0.012
ζ (%)	1	0.427	0.389	8.875	0.429	0.441
	2	0.471	0.511	8.438	0.471	0.025
	3	0.312	0.279	10.601	0.321	2.732
	4	0.551	0.493	10.476	0.545	1.113
	5	0.447	0.444	0.603	0.449	0.434

as indicated by dashed lines in Figure 16(b). The initialization of the center frequencies $\{\omega_k^1\}$ in VMD is thus realized as $\{\omega_k^1\} = \{15.4, 19.0, 28.4, 45.4, \text{and } 55.6\,\text{Hz}\}$. Apparently, the number of modes K is 5. The optimized value of α through GA is 1.31e5 in this case. Nevertheless, some state-of-the-art optimization algorithms such as particle swarm optimization (PSO), simulated annealing (SA), and immune algorithm (IA) could also be utilized to search for the optimal value of α while no significant impact on the outcome has been found by the author.

The extracted modes and the corresponding Fourier spectra are depicted in Figure 17 where obviously each component contains a single oscillation mode. Despite the boundary issues, the Hilbert spectrum as shown in Figure 18 further demonstrates that the frequency pattern is successfully captured without overbinning or underbinning. The modal information of the extracted modes is derived by Hilbert transform and detailed in Table 3. With the purpose of comparison, the PolyMAX method in the frequency domain is also employed to identify the modal parameters of the low-pass filtered test data. The results are also listed in Table 3 and the stabilization diagram is plotted in Figure 19.

Compared with the theoretical values calculated via the finite element method (FEM), the first five modal frequencies of a single test identified are quite accurate for both methods where all the percentage errors are within 0.2%. However, the performance of the two methods on the identification of the damping ratio differs greatly. The identification errors of the proposed method are dramatically small with the maximum value within 3%. The PolyMAX identification in the frequency domain behaves relatively badly for the vibration test. Again, the experimental results demonstrate the effectiveness of the proposed method in the separation of modes and recovering the most modal information at the same time.

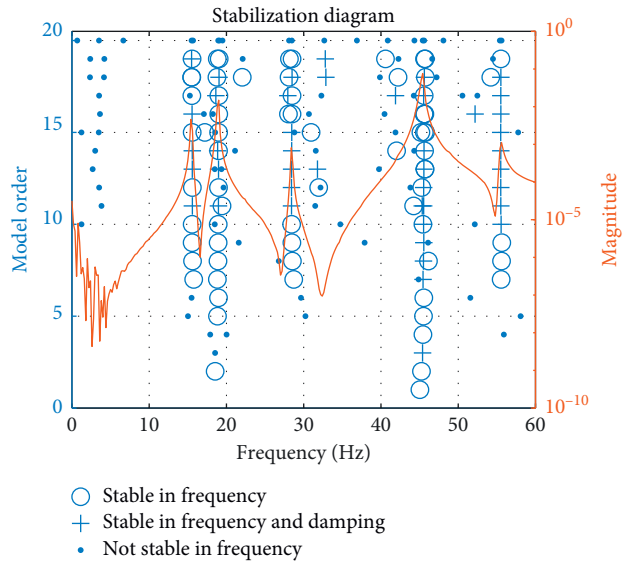

Figure 19: Stabilization diagram utilizing PolyMAX identification in the frequency domain.

4. Conclusions

In this paper, the equivalent filter characteristics of VMD are studied when applied to the fGn, and the application in the separation of closely spaced modes of vibration system is performed. Extensive numerical simulations have been carried out and demonstrated the differences in filter performance between VMD and EMD.

Contrary to EMD, the VMD possesses the filter characteristics similar to WPT with almost identical bandwidth. Moreover, the initialization along with the constraint parameter α does have a great impact on the decomposition performance of VMD. For a small value of α, the self-adaptability of VMD is recovered. In addition, regardless of the initialization, the spectral characteristics of the inspected signal are successfully captured. Meanwhile, the increase of α reinforces the linear relationship between the initial center frequencies and the converged frequencies. In other words, the algorithm is forced to converge to the local minimum in the case of a large value of α. Taking advantage of the filter performance, criteria for the optimization of α and the initialization of center frequencies $\{\omega_k^1\}$ are established to extract a desired collection of modes. Center frequencies are to be initialized by the prior identified modal frequencies utilizing the simple peak-picking method, whereas the value of α is optimized through GA based on the proposed fitness function. Both numerical simulations and experimental tests have demonstrated the capability of the proposed method based on VMD in the separation of modes while retaining the most modal information at the same time. However, the presented optimized VMD adds an extra requirement which greatly increases the computational cost. Considering the accuracy of the identified closely spaced modes, however, the presented optimized VMD could be applied in engineering practice, whereas the compared methods lose their validity in the same situation.

Although all the analyzed response signals in this paper are obtained under impulse excitation, for random responses, techniques like random decrement technique (RDT) and natural excitation technique (NeXT) could be used to extract the free decaying response and thus complete the applicability of the proposed method.

Data Availability

The data used to support the findings of this study are available from the corresponding author upon request.

Conflicts of Interest

The authors declare that there are no conflicts of interest regarding the publication of this paper.

Acknowledgments

This research was partially supported by the National Natural Science Foundation of China (Grant no. 51475228), the Priority Academic Program Development of Jiangsu Higher Education Institutions, and the Postgraduate Research & Practice Innovation Program of Jiangsu Province (KYCX19_0153).

References

[1] N. E. Huang, Z. Shen, S. R. Long et al., "The empirical mode decomposition and the Hilbert spectrum for nonlinear and non-stationary time series analysis," *Proceedings Mathematical Physical & Engineering Sciences*, vol. 454, no. 1971, pp. 903–995, 1998.

[2] N. E. Huang and S. S. P. Shen, *Hilbert-huang Transform and its Applications*, World Scientific, Singapore, 2005.

[3] Z. K. Peng, P. W. Tse, and F. L. Chu, "An improved Hilbert-Huang transform and its application in vibration signal analysis," *Journal of Sound and Vibration*, vol. 286, no. 1-2, pp. 187–205, 2005.

[4] M. Amarnath and I. R. Praveen Krishna, "Local fault detection in helical gears via vibration and acoustic signals using EMD based statistical parameter analysis," *Measurement*, vol. 58, pp. 154–164, 2014.

[5] X. H. He, X. G. Hua, Z. Q. Chen, and F. L. Huang, "EMD-based random decrement technique for modal parameter identification of an existing railway bridge," *Engineering Structures*, vol. 33, no. 4, pp. 1348–1356, 2011.

[6] J. Chen, Y. L. Xu, and R. C. Zhang, "Modal parameter identification of Tsing Ma suspension bridge under Typhoon Victor: EMD-HT method," *Journal of Wind Engineering and Industrial Aerodynamics*, vol. 92, no. 10, pp. 805–827, 2004.

[7] Z. Wu and N. E. Huang, "Ensemble empirical mode decomposition: a noise-assisted data analysis method," *Advances In Adaptive Data Analysis*, vol. 1, no. 1, pp. 1–41, 2009.

[8] J.-R. Yeh, J.-S. Shieh, and N. E. Huang, "Complementary ensemble empirical mode decomposition: a novel noise enhanced data analysis method," *Advances in Adaptive Data Analysis*, vol. 2, no. 2, pp. 135–156, 2010.

[9] M. A. Colominas, G. Schlotthauer, and M. E. Torres, "Improved complete ensemble EMD: a suitable tool for biomedical signal processing," *Biomedical Signal Processing and Control*, vol. 14, pp. 19–29, 2014.

[10] Z. Wu and N. E. Huang, "A study of the characteristics of white noise using the empirical mode decomposition

method," *Proceedings of the Royal Society A: Mathematical, Physical and Engineering Sciences*, vol. 460, no. 2046, pp. 1597–1611, 2004.

[11] H. Li, Z. Li, and W. Mo, "A time varying filter approach for empirical mode decomposition," *Signal Processing*, vol. 138, pp. 146–158, 2017.

[12] J. Yang, P. Li, Y. Yang, and D. Xu, "An improved EMD method for modal identification and a combined static-dynamic method for damage detection," *Journal of Sound and Vibration*, vol. 420, pp. 242–260, 2018.

[13] K. Dragomiretskiy and D. Zosso, "Variational mode decomposition," *IEEE Transactions on Signal Processing*, vol. 62, no. 3, pp. 531–544, 2014.

[14] C. Yi, Y. Lv, and Z. Dang, "A fault diagnosis scheme for rolling bearing based on particle swarm optimization in variational mode decomposition," *Shock and Vibration*, vol. 2016, Article ID 9372691, 10 pages, 2016.

[15] X. Wang, Z. Yang, and X. Yan, "Novel particle swarm optimization-based variational mode decomposition method for the fault diagnosis of complex rotating machinery," *IEEE/ASME Transactions on Mechatronics*, vol. 23, no. 1, pp. 68–79, 2018.

[16] S. Fei, "The hybrid method of VMD-PSR-SVD and improved binary PSO-KNN for fault diagnosis of bearing," *Shock and Vibration*, vol. 2019, Article ID 4954920, 7 pages, 2019.

[17] Z. Lv, B. Tang, Y. Zhou, and C. Zhou, "A novel method for mechanical fault diagnosis based on variational mode decomposition and multikernel support vector machine," *Shock and Vibration*, vol. 2016, Article ID 3196465, 11 pages, 2016.

[18] P. Zhang and J. Zhang, "Application of variational mode decomposition and k-Nearest neighbor algorithm in the quantitative nondestructive testing of wire ropes," *Shock and Vibration*, vol. 2019, Article ID 9828536, 14 pages, 2019.

[19] T. Han and D. Jiang, "Rolling bearing fault diagnostic method based on VMD-AR model and random forest classifier," *Shock and Vibration*, vol. 2016, Article ID 5132046, 11 pages, 2016.

[20] B. Xu, H. Li, F. Zhou, and B. Yan, "Fault diagnosis of variable load bearing based on quantum chaotic fruit fly VMD and variational RVM," *Shock and Vibration*, vol. 2019, Article ID 8213056, 20 pages, 2019.

[21] Y. Wang, R. Markert, J. Xiang, and W. Zheng, "Research on variational mode decomposition and its application in detecting rub-impact fault of the rotor system," *Mechanical Systems and Signal Processing*, vol. 60-61, pp. 243–251, 2015.

[22] Y. Liu, G. Yang, M. Li, and H. Yin, "Variational mode decomposition denoising combined the detrended fluctuation analysis," *Signal Processing*, vol. 125, pp. 349–364, 2016.

[23] S. Hu, H. Xiao, and C. Yi, "A novel detrended fluctuation analysis method for gear fault diagnosis based on variational mode decomposition," *Shock and Vibration*, vol. 2018, Article ID 7045127, 11 pages, 2018.

[24] M. R. A. Paternina, R. K. Tripathy, A. Z. Mendez, and D. Dotta, "Identification of electromechanical oscillatory modes based on variational mode decomposition," *Electric Power Systems Research*, vol. 167, pp. 71–85, 2019.

[25] J. A. de la O Serna, J. M. Ramirez, A. Zamora Mendez, and M. R. A. Paternina, "Identification of electromechanical modes based on the digital Taylor-Fourier transform," *IEEE Transactions on Power Systems*, vol. 31, no. 1, pp. 206–215, 2016.

[26] S. Chen, Y. Yang, Z. Peng, X. Dong, W. Zhang, and G. Meng, "Adaptive chirp mode pursuit: algorithm and applications," *Mechanical Systems and Signal Processing*, vol. 116, pp. 566–584, 2019.

[27] S. Chen, Y. Yang, Z. Peng, S. Wang, W. Zhang, and X. Chen, "Detection of rub-impact fault for rotor-stator systems: a novel method based on adaptive chirp mode decomposition," *Journal of Sound and Vibration*, vol. 440, pp. 83–99, 2019.

[28] G. Yu, M. Yu, and C. Xu, "Synchroextracting transform," *IEEE Transactions on Industrial Electronics*, vol. 64, no. 10, pp. 8042–8054, 2017.

[29] S. Wang, X. Chen, C. Tong, and Z. Zhao, "Matching synchrosqueezing wavelet transform and application to aero-engine vibration monitoring," *IEEE Transactions on Instrumentation and Measurement*, vol. 66, no. 2, pp. 360–372, 2017.

[30] Z. Feng, X. Chen, and M. Liang, "Iterative generalized synchrosqueezing transform for fault diagnosis of wind turbine planetary gearbox under nonstationary conditions," *Mechanical Systems and Signal Processing*, vol. 52-53, pp. 360–375, 2015.

[31] B. B. Mandelbrot and J. W. Van Ness, "Fractional Brownian motions, fractional noises and applications," *SIAM Review*, vol. 10, no. 4, pp. 422–437, 1968.

[32] P. Flandrin, P. Gonçalvès, and G. Rilling, "EMD equivalent filter banks, from interpretation to applications," in *Hilbert -Huang Transform and its Applications*, N. E. Huang and S. S. P. Shen, Eds., pp. 57–74, World Scientific, Singapore, 2005.

[33] P. Flandrin, G. Rilling, and P. Goncalves, "Empirical mode decomposition as a filter bank," *IEEE Signal Processing Letters*, vol. 11, no. 2, pp. 112–114, 2004.

[34] A. T. A. Wood and G. Chan, "Simulation of stationary Gaussian processes in [0, 1] d," *Journal of Computational and Graphical Statistics*, vol. 3, no. 4, pp. 409–432, 1994.

[35] J. Zeng and S. L. Kukreja, "Flutter prediction for flight/wind-tunnel flutter test under atmospheric turbulence excitation," *Journal of Aircraft*, vol. 50, no. 6, pp. 1696–1709, 2013.

[36] Y.-H. Wang, C.-H. Yeh, H.-W. V. Young, K. Hu, and M.-T. Lo, "On the computational complexity of the empirical mode decomposition algorithm," *Physica A: Statistical Mechanics and Its Applications*, vol. 400, pp. 159–167, 2014.